Am J Transl Res 2021;13(8):8873-8884
www.ajtr.org /ISSN:1943-8141/AJTR0132037

Original Article

Molecular photoacoustic imaging for early diagnosis and treatment monitoring of rheumatoid arthritis in a mouse model

Yimu Lin[1], Shuyi Xiao[2], Wei Yao[3], Zhuang Lv[4], Yufu Tang[5], Yu Zhang[1], Liang Chen[1]

[1]Department of Orthopedics, The Second Affiliated Hospital and Yuying Children's Hospital of Wenzhou Medical University, Wenzhou 325000, P. R. China; [2]Sir Run Run Shaw Hospital, College of Medicine, Zhejiang University, Hangzhou 310016, P. R. China; [3]Department of Respiratory Medicine, Huzhou First People's Hospital, Huzhou 313000, P. R. China; [4]Key Laboratory for Organic Electronics and Information Displays, Institute of Advanced Materials (IAM), Jiangsu National Synergetic Innovation Center for Advanced Materials (SICAM), Nanjing University of Posts and Telecommunications (NUPT), Nanjing 210023, P. R. China; [5]Key Laboratory of Flexible Electronics (KLOFE), Institute of Advanced Materials (IAM), Jiangsu National Synergetic Innovation Center for Advanced Materials (SICAM), Nanjing Tech University (Nanjing Tech), Nanjing 211816, P. R. China

Received February 18, 2021; Accepted June 11, 2021; Epub August 15, 2021; Published August 30, 2021

Abstract: Rheumatoid arthritis (RA) is a progressive inflammatory joint disease. Early diagnosis is critical for timely therapeutic intervention. However, it lacks effective diagnostic methods capable of detecting disease progression in its early stage and evaluating treatment efficacy in clinics. Photoacoustic (PA) molecular imaging is a novel imaging modality that can detect in the early stage of disease and continuously monitor its progression. In this study, Evans blue (EB) was used as a PA contrast agent to detect the angiogenesis and microcirculation dysfunction in RA joint. In collagen-induced arthritis (CIA) mouse model, a distinct increase of PA signal was detected early at 2 weeks, with significant higher PA signal intensities from the RA joints compared to the normal joints. More importantly, we detected an increasing trend of PA signal intensity week by week post CIA induction, demonstrating the potential of EB-enhanced PA imaging in monitoring the development of RA. However, joint damage was silent in the X-ray at 2 weeks post CIA induction, which suggested the superiority of PA imaging in RA early detection. In addition, striking decrease of PA signal intensities in the RA joints was observed after administration with etanercept compared with the untreated RA joints. The signal changes exhibited by PA imaging were confirmed by clinical observation and histological examinations. This study demonstrated the promising use of EB-enhanced PA imaging for the early diagnosis and its feasibility for RA treatment monitoring.

Keywords: Rheumatoid arthritis, Evans blue, photoacoustic molecular imaging, diagnosis, disease progression, treatment monitoring

Introduction

Rheumatoid arthritis (RA) is a systemic autoimmune inflammatory disorder, characterized by synovium inflammation, resulting in significant disability and high socioeconomic costs [1, 2]. About 80% of RA patients are disabled after 20 years. Improvement of the clinical outcomes for patients with RA and timely intervention and optimal adjustments of therapies rely on techniques for early diagnosis and sensitively monitoring disease progression [3, 4]. However, patients clinically diagnosed with RA are commonly in an advanced stage for which disease-modifying opportunities are limited [5].

Currently, it lacks effective imaging modalities capable of diagnosing early RA or monitoring efficacy of treatments. In clinics, routine X-ray is the most commonly applied imaging modality in assessing RA, however, it can only exhibit advanced bone destruction years after the initial inflammation [6]. Magnetic resonance imaging (MRI) is more sensitive for soft tissues and bone erosions but not suitable for routine use because of economic and location limitations

[7]. Ultrasound is more conducive than conventional X-ray in soft tissue imaging, and is being used more extensively, as it is relatively cheap, accessible, and non-ionizing. However, because of its limited sensitivity in inflammatory tissue, ultrasound is not suitable as a primary imaging tool for this inflammatory arthritis disease [8]. Consequently, powerful non-invasive preclinical imaging techniques, especially those that can detect RA before its reversible stage, are therefore highly desirable.

Molecular imaging visualizes, detects and quantifies molecule biomarkers in diseases such as cancer or RA [9, 10]. It paves the way to provide information on biomarkers, cells, and pathways, which improves diagnosis accuracy as well as personal therapeutic guidance. Photoacoustic (PA) imaging is a novel hybrid imaging method, providing powerful endogenous optical absorption contrasts with high resolution [11-13]. It is an ideal molecular imaging technique for *in vivo* applications because of its deeper imaging depth. With knowledge of the optical absorbance, PA imaging has succeeded in providing physiological and pathological information at molecular level [14, 15]. Besides, PA imaging is much safer than X-ray. Thus, it has been widely used in various applications in biomedical field, including brain imaging, cardiovascular diseases monitoring, as well as the evaluation of cancer detecting efficiency [16-19]. Applied to bone and joint imaging, PA imaging has demonstrated anatomical visualization of the normal human peripheral joints [20-22].

In order to enhance PA signal from deep tissues, the use of a biocompatible contrast agent is attractive. Evans blue (EB) is a non-toxic azo dye with high hydrophilicity and slow excretion. Owning to its high binding affinity to serum, EB has been broadly used for biomedical applications [23]. As a desirable PA agent, EB has high absorption coefficient in the main wavelength region of spectrum, with a weak peak at 680 nm, used for PA imaging [24]. The strong binding property of EB to serum albumin leads to its broad applications in biomedicine, in particular, its use in the detection of leakage through blood vessels in the blood-tissue barriers including the blood-brain barrier, blood-retinal barrier and blood-testis barrier [25-27]. The fact that EB-albumin macromolecule is confined to the blood vessels under physiologic conditions makes EB unique among other dyes. Free EB dye is more likely to diffuse into the extravascular tissues, which will be cleared by metabolism or excretion finally. When there is a disruption of barrier and enhanced vascular permeability, EB-albumin macromolecule will diffuse from the circulation into neighboring tissues, which in turn enables microcirculation damage. Angiogenesis accompanied by inflammation leads to the dysfunction of blood-joint barrier in RA-inflamed joints, which further results in enhanced permeability [28, 29]. Additionally, the metabolism demand of synoviocytes is upregulated, and arthritic joints require more albumin as a relevant energy source than healthy tissues [30]. Thus, the accumulation of albumin in inflamed tissues in RA is an important molecular biomarker for RA diagnosis and therapeutic monitoring [30].

In this study, we used EB as a PA probe to investigate the superiority of PA imaging in visualizing angiogenesis and the increased vascular permeability in collagen-induced arthritis (CIA) mice to diagnose and monitor the treatment of RA progression. To further verify the parallel diagnostic outcome of PA imaging, X-ray examination was conducted on the same mice. By comparing the PA imaging results with the X-ray results and pathological examinations of foot joint, our study exhibited that EB-enhanced PA imaging was reliable enough, if adapted to clinical practice, to help in diagnosing RA in its early stage, and therefore facilitate therapeutic options.

Materials and methods

Ethics statement

All experiments were approved by the Institutional Animal Care and Use Committee of Wenzhou Medical University. The animal procedures were carried out strictly according to institutional and national guidelines. Fifty male Kunming mice with body weights of 30 g were obtained from the experimental animal center of Wenzhou Medical University (wydw2020-0582); 4-5 mice were housed in a conventional cage, which was kept in a room with constant 21°C room temperature as well as 45% humidity, under controlled 12 h light-dark lighting cycle. The mice were allowed free access to water and standard food.

Animal model

CIA mouse model established by a double immunization was used in this study according to previous studies [24, 31]. In brief, equal volumes of complete Freund's adjuvant (4 mg/mL) and type II bovine collagen solution (2 mg/mL) were injected subcutaneously into the mice paw for the first immunization. At 21 days after the first immunization, a booster immunization of incomplete Freund's adjuvant emulsified with bovine type-II collagen was given to the mice. The mice were anesthetized under 2% isoflurane and anesthesia was maintained during the adjuvant injection and imaging experiment. To examine the feasibility of PA imaging in RA diagnosis, 5 foot joints from the RA mice were imaged at 0, 2 and 4 weeks after RA induction and compared with the 8 healthy joints in the control group. In addition, the mice were monitored every few days. The change of paw thickness from baseline during experiment was monitored. Clinical arthritic scores were scored according to a previous study [32].

Photoacoustic imaging system characterization

Endra Nexus 128 PA scanner system was applied for PA imaging (AnnArbor, MI). The laser wavelength was tunable from 680 to 950 nm (at the repetition rate of 20 Hz and pulse width of 7 ns). The laser output energy from the source was well below 20 mJ/cm^2 per pulse, meeting the safety standard of American National Standard Institute (ANSI) [33]. The PA waves were detected by an ultrasound transducer, creating an image of the optical absorption distribution inside the tissues and transmitting to the computer. In this study, PA images were acquired under 680 nm laser wavelength. Before imaging the foot joint, hair on the mouse paw was completely removed to avoid light blockage. Then the imaged target (foot) was well mounted on the protruding tip of the bowl. The imaged position remained consistent to narrow the imaging difference. The protruding tip of the bowl was immersed in water and the interface between the slot and imaging target did not have bubbles. Software OsiriX Lite (OsiriX Foundation, Genève, Switzerland) was applied to analyze the reconstructed raw data, and the quantitative PA signal intensity of region of interesting (ROI) was measured by OsiriX Lite.

In vivo PA imaging and data analysis

In this study, low concentration (0.5 wt%) of EB, which is mainly the EB-albumin that diffuses out of the blood vessels, was used as the PA contrast agent. A phosphate-buffered saline (PBS, pH=7.5) solution of EB (Sigma) at a concentration of 0.5 wt% was intravenously injected into the dorsal veins of the tail at the dose of 2.5 mg/kg body weight. The mice were anesthetized under 2% isoflurane and adjusted to maintain a surgical plane of anesthesia during the adjuvant injection and imaging procedure. All animals were imaged by the PAI system at 680 nm wavelength from 0-24 h post-injection of the EB probes. To examine the feasibility of EB-enhanced PA imaging in RA diagnosis, 5 foot joints from the RA mice were imaged at 0, 2 and 4 weeks after CIA induction and compared with the 5 healthy joints from the control group. The ROI (10 mm × 8 mm, indicated by a white dashed rectangle) was drawn over each sample on the PA images and the mean PAI intensity was measured by OsiriX imaging system software package. Through all stages of the imaging procedure, respiration rate and signs of distress were monitored.

X-ray of mice foot joint

To further verify the diagnostic outcome of PAI, in parallel, X-ray examination was performed on the same mice. The mice were anesthetized under 2% isoflurane and adjusted to maintain a surgical plane of anesthesia during the imaging process. X-ray examinations for all the foot joints at antero-posterior projections were done with X digital imaging system (MX-20, Faxitron, American) for small animal and all the results were evaluated by an experienced radiologist in X-ray imaging of RA.

Monitoring therapeutic response by EB-enhanced PA imaging

To illustrate the feasibility of EB-enhanced PA imaging in assessing the treatment efficacy, RA mice in the treatment group were administered with etanercept (Enbrel®), an anti-tumor necrosis factor medication used in clinical for RA. Starting from the week 2 after CIA induction, each RA mouse was intramuscularly injected with 100 μL of PBS or etanercept (0.3 ml/kg) four times every four days (i.e., treated on day 14, 18, 22, 26, 30, respectively). At week 6, the

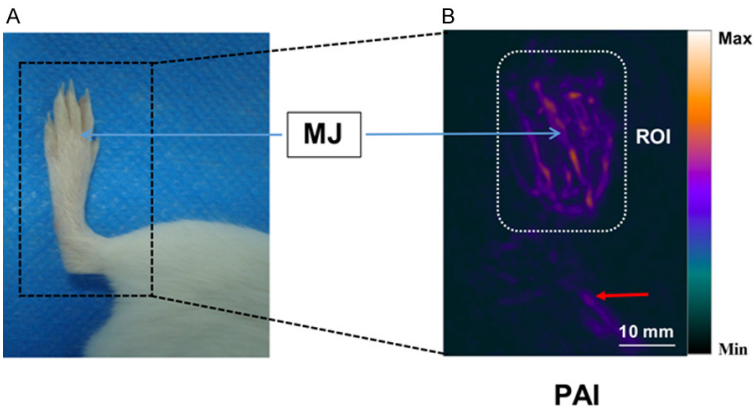

Figure 1. PA imaging at 680 nm of a normal mouse paw. A. Optical photograph of mouse foot. B. PA image of mouse paw. The blue arrow indicated the metatarsophalangeal joint (MJ). The red arrow indicated the anterior tibial vessels. Scale bar: 10 mm.

foot joints of control group (treated with PBS) and etanercept-treated group were imaged.

Histological analysis

After *in vivo* imaging, the mice were euthanized with carbon dioxide. Paws were isolated and fixed in 4% paraformaldehyde for 24 hours. Then they were decalcified in 10% EDTA for 6 days and embedded in paraffin. Serial sections were cut 5 μm for each section sagittally across the metatarsophalangeal joints at 40 μm intervals. Slides were stained with hematoxylin and eosin (H&E) staining. A board-certified veterinary pathologist evaluated H&E stained slides. Additionally, vascular endothelial growth factor (VEGF) staining (Wuhan GoodBiosciences, Wuhan, China) was used as a further index of the angiogenesis.

Statistical analysis

The OsiriX imaging system software package was used to analyze the data of PA signal intensities in ROI. All data were given as the mean ± standard deviation (S.D.). Data were processed by using GraphPad software (GraphPad Software, Inc., La Jolla, CA, Version 6.0d) and analyzed by the Student's t-test or one-way ANOVA. Statistical significance was considered as for *P* values of <0.05.

Results

Increased PA signal intensity in RA joint after EB injection

The photographic and PA images of a healthy foot joint are shown in **Figure 1**. In the PA images, due to the intrinsic chromophores of hemoglobin and calcium in bone of mice foot, the metatarsophalangeal joints (MJs) were presented, and we could recognize the anatomical structure of the foot, which also enabled us to select a region of interest (ROI, 10 mm × 8 mm, indicated in the white dashed rectangle). However, without additional contrast agent, the average PA intensity collected from the desired region was 495±73, primarily generated from calcium and hemoglobin.

Two weeks after CIA induction, the mice were injected with EB and serially PA imaged within 24 h. Representative PA images are shown in **Figure 2A**. In the normal foots, an increase of PA signal confined in the blood vessels was detected at 0.5 h after EB injection, but it soon decreased to the baseline level (about 12 h). The time interval, 0.5 h, post EB injection was chosen for the following image time point. Besides, a much stronger PA signal intensity was observed in RA joint than the normal one at 0.5 h post injection ($P<0.01$). It was maximized to 2247±95 at 0.5 h, which was 2.56-fold that of the injection at 0 h (**Figure 2B**). Additionally, the retention half-life of EB-albumin complex in RA joints was 12 h, which was significantly longer than the 3 h retention half-life of normal joints ($P<0.01$). Further analysis of the PA intensity ratios between RA and normal joints after injection was as follows: 0.5 h after injection was 2.42, and 24 h after injection was 1.28, indicating that the cumulative effect of EBA between RA and normal joints was significantly different (**Figure 2C**).

EB-albumin sensitive PA signal intensity steadily increases over RA progression in mice

Compared with normal controls, the observation that EB-albumin complex-sensitive PA signal was significantly higher in RA joint led us to hypothesize that PA signal intensity might be correlated with RA development as the inflammation increased. In **Figure 3**, each mouse was imaged serially every 2 weeks over 4 weeks post RA induction. Strikingly, at every examined time point, the RA foot exhibited a higher PA sig-

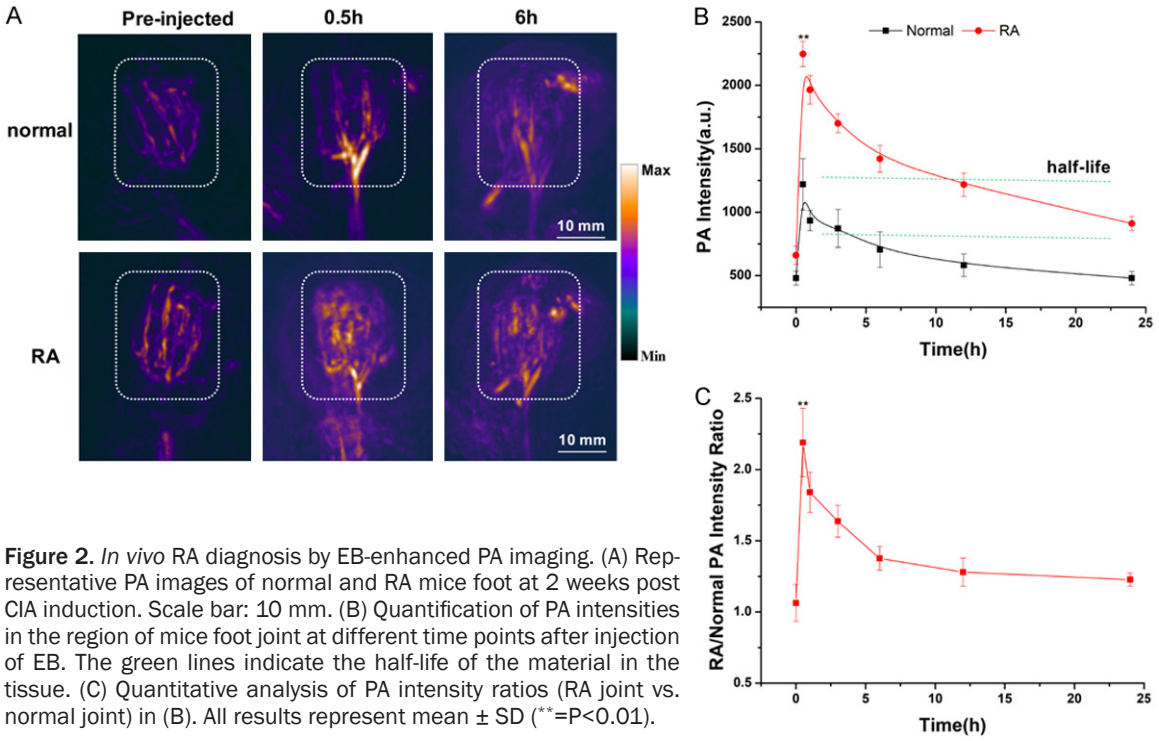

Figure 2. *In vivo* RA diagnosis by EB-enhanced PA imaging. (A) Representative PA images of normal and RA mice foot at 2 weeks post CIA induction. Scale bar: 10 mm. (B) Quantification of PA intensities in the region of mice foot joint at different time points after injection of EB. The green lines indicate the half-life of the material in the tissue. (C) Quantitative analysis of PA intensity ratios (RA joint vs. normal joint) in (B). All results represent mean ± SD (**=P<0.01).

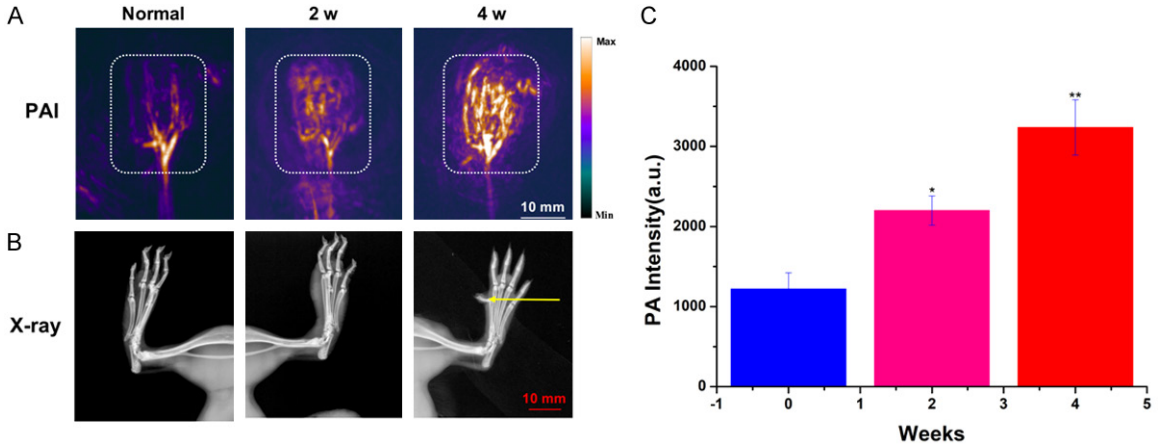

Figure 3. *In vivo* monitoring the development of RA via EB-enhanced PA imaging and X-ray. A. Representative PA images of normal and RA mice foot at different weeks (n=5). All PA images have the same scale bar. Scale bar: 10 mm. B. X-ray of the same mouse foot at the same imaging time points with PA imaging. The red circle contained the pathologically altered mouse foot at 4 weeks. The yellow arrow indicated bone destruction and narrowed joint space in the metatarsophalangeal joint. All X-ray images have the same scale bar. Scale bar: 10 mm. C. Mean PA intensity collected from each mouse knee, quantified from collected PA images. All results represent mean ± SD (*=P<0.05, **=P<0.01).

nal than the normal foot, which received the same number of injections as the RA mice (**Figure 3A**). Signal quantification showed that the average PA intensity of the RA foot increased linearly from 0 to 4 weeks post CIA induction, while signals of normal foot only increased slightly over time (**Figure 3C**). This data indicated that the EB-albumin leaked from the RA joints shortly after induction and continuously rose from the very early stage of RA to moderate RA.

The symptoms remained silent in the X-ray detection at 2 weeks (**Figure 3B**), such as nar-

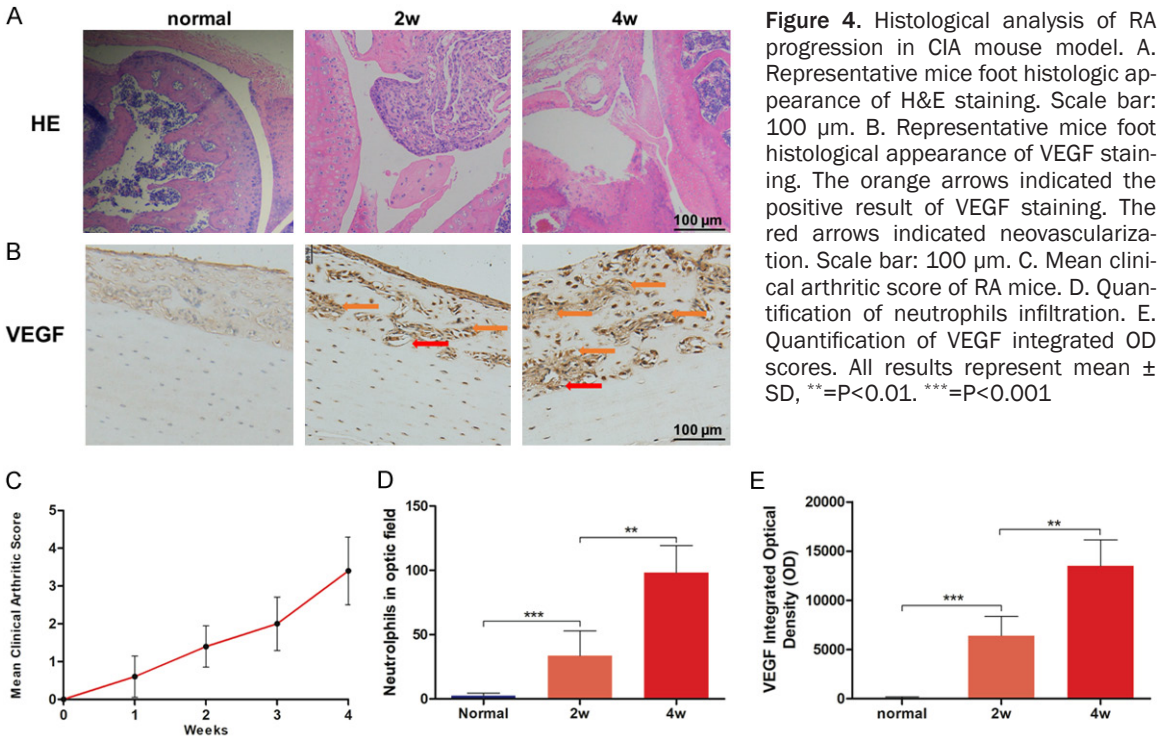

Figure 4. Histological analysis of RA progression in CIA mouse model. A. Representative mice foot histologic appearance of H&E staining. Scale bar: 100 μm. B. Representative mice foot histological appearance of VEGF staining. The orange arrows indicated the positive result of VEGF staining. The red arrows indicated neovascularization. Scale bar: 100 μm. C. Mean clinical arthritic score of RA mice. D. Quantification of neutrophils infiltration. E. Quantification of VEGF integrated OD scores. All results represent mean ± SD, **=P<0.01. ***=P<0.001

rowed joint space (sign of bone remodeling and cartilage loss), juxta-articular osteoporosis and bone destruction. In the X-ray (**Figure 3B**), we could see mild bone destruction and joint space narrowing in the MJs (yellow arrows) at 4 weeks. It should also be highlighted that the size of mice foot gradually expanded in PA images during RA progression. This may be related to the swelling and proliferation during RA.

Histopathologic findings

We further conducted clinical and histological analyses to examine the pathological severity of MJs. The feet of the CIA mice were assigned clinical scores on a scale ranging from 0 to 5 that reflected the severity of inflammation and swelling. In **Figure 4C**, the mean clinical arthritic scores were gradually raised along with the progression of RA post CIA induction. As shown in **Figure 4A** and **4D**, when compared with normal joint, the joint of RA foot exhibited prominent neutrophil infiltration, cartilage erosion, and synovial inflammation at 2 and 4 after CIA induction. At 2 weeks after CIA induction, there were no obvious osseous structural changes in the RA foot joint, such as narrowed joint space or osteophyte. While in the 4 weeks group, we can see more severe cartilage lesion and mild bone destruction. In **Figure 4B**, a remarkable increase of new blood vessels around the joint was shown in immunohistochemical staining at 2 weeks and was much more evident at 4 weeks post CIA induction. In addition, quantification of immunohistochemical staining revealed the increased VEGF expression in RA joints along with the development of synovitis (**Figure 4E**, P<0.001, P<0.01, respectively).

Treatment efficacy monitoring

EB-enhanced PA imaging was then tested for efficacy of the biological agent etanercept in real time *in vivo* and to discover whether it prevents the progression of joint destruction as a potential disease-modifying anti-rheumatic drug (DMARD). The mice were intramuscularly administrated with etanercept at 2 weeks post CIA induction. At 6 weeks, the RA foot joints of the etanercept-treated and control group were imaged to assess the therapeutic efficacy. Representative images (posteroanterior and lateral position) from both groups are shown in **Figure 5A**. With five joints in each group, the average PA signal intensities are presented in **Figure 5B**. In comparison to the non-treatment group, dramatically decreased PA intensities of

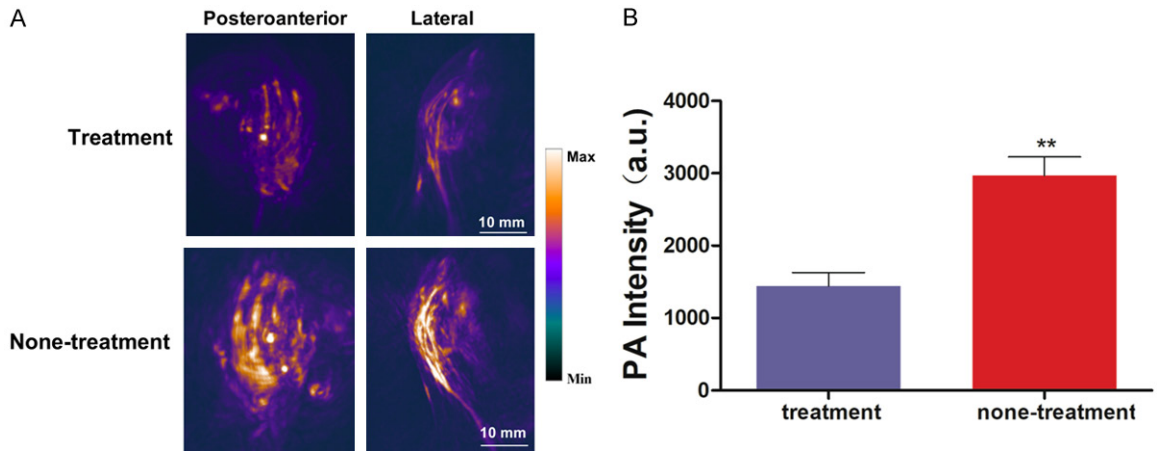

Figure 5. Therapeutic monitoring ability of EB-enhanced PA imaging in RA. A. Representative PA images of RA mice foot with different imaging position compared between etanercept-treated mice and non-treated mice (n=5). Scale bar: 10 mm. B. Quantification of PA intensity collected from etanercept-treated mice and non-treated mice. All results represent mean ± SD, **=P<0.01 (n=5).

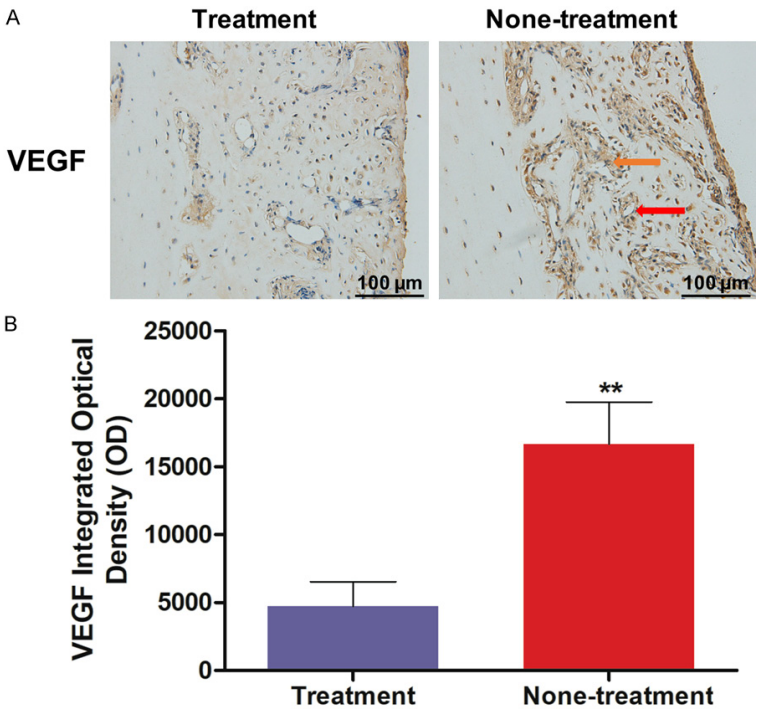

Figure 6. Immunohistochemical analysis of therapeutic efficacy of etanercept. A. Immunohistochemical staining of VEGF. The orange arrow indicated the positive result of VEGF staining. The red arrow indicated neovascularization. Scale bar: 100 μm. B. Quantification of VEGF integrated OD scores. All results represent mean ± SD, **=P<0.01.

joints were detected in the treatment group (*P*<0.01). VEGF staining exhibited strongly positive results in the interstitial space of muscle tissue in the non-treatment group (**Figure 6A**). RA mice treated with etanercept showed relatively reduced bone erosion and cartilage degeneration, and the prominent inflammatory cell infiltration in the joints was also reduced. Using immunohistochemistry to quantify VEGF expression, we observed remarkably less expression of VEGF in the treatment group (**Figure 6B**), suggesting that evaluating the angiogenesis and microcirculation damage in synovial tissues through PA imaging paves the way to monitoring the treatment efficacy of RA (*P*<0.01).

Discussion

Identification of biomarkers is beneficial for detecting early disease, monitoring disease progression, and assessing treatment responses, which is also a priority for RA research as it represents a major obstacle to progress for the improvement of disease modifying RA drugs [34-36]. Currently, diagnosing and monitoring RA progression in animals largely rely on histological analysis in preclinical research [37]. Histopathological examination is invasive and is unable for long-term monitoring and evaluating therapeutic respons-

es. Novel imaging modalities combined with specific disease biomarkers will help solve these problems [38, 39]. This study demonstrated that the increased microcirculation disorder in RA foot joints of mice can be detected with EB-enhanced PA imaging techniques. Therefore, the non-invasive EB-enhanced PA imaging may facilitate an early and continuous observation over the course of RA development, which can be further applied in patients' responses to the therapy.

In the progression of RA, angiogenesis and increased permeability is noted in and around the synovium within the affected joints. Following an initial insult, vasodilatation occurs rapidly, additional capillaries are recruited, and the permeability of these capillaries is subsequently enhanced. Microcirculatory permeability can be divided into immediate phase (endothelial cell contraction), transient response (endothelial injury) and transcytosis.

The ensuing macromolecular (such as albumin) extravasation contributes to joint swelling. In addition, the chronicity of local inflammation, accompanied by continuous angiogenesis and ongoing remodeling, provides opportunities for the accumulation of macromolecules. Hence, imaging and quantifying albumin potentially enable objectively assess RA progression and its degree. EB is nontoxic and can be used to measure blood volume [40], lymph node location [41], microvascular permeability [42], blood-retinal barrier destruction [43], capillary perfusion [44], and blood plasma flow [45], among other applications. In the bloodstream, EB mainly binds to serum albumin in a reversible manner, so it is uniformly distributed in the plasma, thereby obtaining a complete capillary network image to the greatest extent.

Our study was implemented under baseline conditions, under which blood vessels were resistant to albumin leakage, so a relatively high EB concentration was used here to detect the microvascular permeability. Moreover, the clearance kinetics of the EB-albumin can be used to estimate the albumin metabolic rate in target tissue [46].

In this study, the raised demand of albumin was remarkably accumulated around the affected joints in the early stage of RA leading to an increase in regional EB-albumin concentration. Enhanced optical absorption had been observed in peri- and intra-articular tissue of the RA joints compared with the normal joints. In our study, compared to the normal joints, RA joints exhibited increased PA signal intensities in the early stage of RA (2 weeks after CIA induction). Furthermore, compared with conventional optical imaging, PA imaging is able to obtain richer anatomical details because of its sufficient spatial resolution [47]. Imaging the EB-albumin with high spatial resolution particularly benefited the study of small joint structures of human hands and foot, which occurred in the initial stage of RA. Our data indicated that the leakage of EB-albumin in the joint occurred shortly after RA induction and continuously rose from the very early stages of RA to moderate RA. Given the lack of understanding and monitoring methods for early RA, it was particularly exciting to observe an increasing trend of total PA signal week to week. However, X-ray only detected mild bone destruction and joint space narrowing at 4 weeks post CIA induction. This illustrates that the standard radiological examination is not sensitive enough for detecting early stage of RA.

We monitored the mice every few days after induction of CIA. The morphology changes of RA mice paws did not show statistical difference from normal paws at 2 weeks, indicating the limitation of clinical observation. Besides, it also strongly proves the superiority of PA imaging in detecting early stage of RA. PA imaging documented a dramatic difference in size of foot segments between the two groups. In the RA joints, the observed enlargement of periarticular tissue showed the primary swelling and proliferation in RA. Morphological changes of foot joints and the associated periarticular tissues manifested the degree of inflammation during RA progression. Our results demonstrated that the joint structure was significantly more damage in the RA joint than the normal control. In addition, the PA results were also confirmed in photographs of mice paws as well as the decreased clinical arthritic scores. Our study suggests the favorable capability of PA imaging in presenting the morphology of articular tissues with both high spatial resolution and excellent optical contrast. By histological examination, we found that the neutrophils representing the severity of synovitis significantly infiltrated the joint (**Figure 4**). It was also

observed that the expression of VEGF was gradually up-regulated post CIA induction. VEGF is a well-known angiogenic factor, which is essential for vasculature development. VEGF promotes the formation of new vessels and enhances vessel permeability [48]. The dual activities of VEGF as an endothelial-cell mitogen and a modulator of changes in vascular permeability are of relevance to the pathogenesis of RA [49]. Herein, it was determined that the PA findings were positively correspondent with the immunohistological result revealing the degree of joint destruction as well as the created angiogenesis including capillaries in the RA joints (**Figure 4**). These results suggest that PAI can potentially detect CIA mice *in vivo* and facilitate the observation of blood-joint permeability.

Monitoring the effectiveness of new therapies has been increasingly significant for translating new treatments from benchtop to bedside and for individualized treatment [50, 51]. However, a major hurdle to translate many non-pharmaceutical and novel pharmaceutical therapies into clinical use is unable to accurately evaluate disease progression and response to these therapies [52]. Considering the effect of PA imaging to detect angiogenesis and microcirculation dysfunction in RA joint, we further tested the ability of PA imaging to monitor the therapeutic efficacy of etanercept. Etanercept is a biological DMARD that is commonly used for RA and ankylosing spondylitis (AS) in clinics. In this study, inhibition of RA inflammation by systemic administration of etanercept to mice resulted in an effective suppression of joint destruction even at 6 weeks after CIA induction. By quantification of VEGF expression, it was determined that the angiogenesis was significantly decreased after etanercept treatment. Compared with the pretreatment, PA intensities significantly decreased after etanercept treatment. In the non-treatment group, the prominent inflammatory cell infiltration in joints still could be observed, whereas it was notably reduced after etanercept administration (**Figure 6A**). Our immunohistological result confirmed the antiangiogenic efficacy of etanercept for RA mice, resulting in the repair of blood-joint barrier, which also proved that the EB-enhanced PA signal correlated well with the therapeutic response. These results indicate the strong potential of EB-enhanced PA imaging in non-invasively monitoring the treatment efficacy.

In conclusion, for this initial study, we illustrated that EB-enhanced PA imaging was powerful enough in early diagnosis and treatment monitoring of RA, in view of its outstanding sensitivity in evaluating angiogenesis and microcirculation dysfunction. Considering the rapid clearance of DMARDs by synovial fluid, the prolonged half time of EB in joint cavity (about 12 h in normal joint) may provide DMARDs increased retention time as well as specific target and reduce drug dose *in vivo*. Our results suggest that PA imaging, with its advanced molecular specificity and high spatial resolution, may be well suited as a clinical method to guide accurate treatment of RA.

Acknowledgements

This work was supported by Wenzhou Municipal Science and Technology Bureau (CN) (No. Y20190266); National Natural Science Foundation of China (No. 61905111).

Disclosure of conflict of interest

None.

Abbreviations

RA, Rheumatoid arthritis; MRI, Magnetic resonance imaging; PA, photoacoustic; EB, Evans blue; CIA, collagen-induced arthritis; ANSI, American National Standard Institute; MJs, metatarsophalangeal joints; H&E, hematoxylin and eosin; VEGF, endothelial growth factor; ROI, region of interesting; S.D., standard deviation; DMARD, disease-modifying anti-rheumatic drug; AS, ankylosing spondylitis.

Address correspondence to: Shuyi Xiao, Sir Run Run Shaw Hospital, College of Medicine, Zhejiang University, 3 Qingchun East Road, Hangzhou 310016, China. Tel: +86-18857222565; E-mail: IZZIEX@163.com; Dr. Liang Chen, Department of Orthopedics, The Second Affiliated Hospital and Yuying Children's Hospital of Wenzhou Medical University, 109 Xueyuan West Road, Wenzhou 325027, China. Tel: +86-15825626615; E-mail: breakingsunshine@163.com

References

[1] Haro I and Sanmarti R. Rheumatoid arthritis: current advances in pathogenesis, diagnosis and therapy. Curr Top Med Chem 2013; 13: 697.

[2] Jones G, Nash P and Hall S. Advances in rheumatoid arthritis. Med J Aust 2017; 206: 221-224.
[3] Pisetsky DS. Advances in the treatment of rheumatoid arthritis: costs and challenges. N C Med J 2017; 78: 337-340.
[4] Burmester GR and Pope JE. Novel treatment strategies in rheumatoid arthritis. Lancet 2017; 389: 2338-2348.
[5] Zembrzuska H and Kumar B. Further considerations of the need for integrated mental health treatment in rheumatoid arthritis patients: comment on the review by matcham et al. Arthritis Rheumatol 2019; 71: 1024-1025.
[6] Pfeil A, Haugeberg G, Renz DM, Reinhardt L, Jung C, Franz M, Wolf G and Bottcher J. Digital X-ray radiogrammetry and its sensitivity and specificity for the identification of rheumatoid arthritis-related cortical hand bone loss. J Bone Miner Metab 2017; 35: 192-198.
[7] Peterfy C, DiCarlo J, Emery P, Genovese MC, Keystone EC, Taylor PC, Schlichting DE, Beattie SD, Luchi M and Macias W. MRI and dose selection in a phase II trial of baricitinib with conventional synthetic disease-modifying antirheumatic drugs in rheumatoid arthritis. J Rheumatol 2019; 46: 887-895.
[8] do Prado AD, Staub HL, Bisi MC, da Silveira IG, Mendonca JA, Polido-Pereira J and Fonseca JE. Ultrasound and its clinical use in rheumatoid arthritis: where do we stand? Adv Rheumatol 2018; 58: 19.
[9] Savic LJ, Schobert IT, Peters D, Walsh JJ, Laage-Gaupp FM, Hamm CA, Tritz N, Doemel LA, Lin M, Sinusas A, Schlachter T, Duncan JS, Hyder F, Coman D and Chapiro J. Molecular imaging of extracellular tumor ph to reveal effects of locoregional therapy on liver cancer microenvironment. Clin Cancer Res 2020; 26: 428-438.
[10] Zheng F, Luo S, Ouyang Z, Zhou J, Mo H, Schoonooghe S, Muyldermans S, De Baetselier P, Raes G and Wen Y. NIRF-molecular imaging with synovial macrophages-targeting vsig4 nanobody for disease monitoring in a mouse model of arthritis. Int J Mol Sci 2019; 20: 3347.
[11] Wang LV. Multiscale photoacoustic microscopy and computed tomography. Nat Photonics 2009; 3: 503-509.
[12] Singh MS and Thomas A. Photoacoustic elastography imaging: a review. J Biomed Opt 2019; 24: 1-15.
[13] Steinberg I, Huland DM, Vermesh O, Frostig HE, Tummers WS and Gambhir SS. Photoacoustic clinical imaging. Photoacoustics 2019; 14: 77-98.
[14] Wang LV and Hu S. Photoacoustic tomography: in vivo imaging from organelles to organs. Science 2012; 335: 1458-1462.
[15] Lin CY, Chen F, Hariri A, Chen CJ, Wilder-Smith P, Takesh T and Jokerst JV. Photoacoustic imaging for noninvasive periodontal probing depth measurements. J Dent Res 2018; 97: 23-30.
[16] Stein EW, Maslov K and Wang LV. Noninvasive, in vivo imaging of blood-oxygenation dynamics within the mouse brain using photoacoustic microscopy. J Biomed Opt 2009; 14: 020502.
[17] Qin H, Zhao Y, Zhang J, Pan X, Yang S and Xing D. Inflammation-targeted gold nanorods for intravascular photoacoustic imaging detection of matrix metalloproteinase-2 (MMP2) in atherosclerotic plaques. Nanomedicine 2016; 12: 1765-1774.
[18] Wang P, Ma T, Slipchenko MN, Liang S, Hui J, Shung KK, Roy S, Sturek M, Zhou Q, Chen Z and Cheng JX. High-speed intravascular photoacoustic imaging of lipid-laden atherosclerotic plaque enabled by a 2-kHz barium nitrite raman laser. Sci Rep 2014; 4: 6889.
[19] Mallidi S, Luke GP and Emelianov S. Photoacoustic imaging in cancer detection, diagnosis, and treatment guidance. Trends Biotechnol 2011; 29: 213-221.
[20] Xu G, Rajian JR, Girish G, Kaplan MJ, Fowlkes JB, Carson PL and Wang X. Photoacoustic and ultrasound dual-modality imaging of human peripheral joints. J Biomed Opt 2013; 18: 10502.
[21] Bodolay E, Koch AE, Kim J, Szegedi G and Szekanecz Z. Angiogenesis and chemokines in rheumatoid arthritis and other systemic inflammatory rheumatic diseases. J Cell Mol Med 2002; 6: 357-376.
[22] Balogh E, Biniecka M, Fearon U, Veale DJ and Szekanecz Z. Angiogenesis in inflammatory arthritis. Isr Med Assoc J 2019; 5: 345-352.
[23] Cooksey CJ. Quirks of dye nomenclature. 1. Evans blue. Biotech Histochem 2014; 89: 111-113.
[24] Liu L, Hu F, Wang H, Wu X, Eltahan AS, Stanford S, Bottini N, Xiao H, Bottini M, Guo W and Liang XJ. Secreted protein acidic and rich in cysteine mediated biomimetic delivery of methotrexate by albumin-based nanomedicines for rheumatoid arthritis therapy. ACS Nano 2019; 13: 5036-5048.
[25] Xu Y, He Q, Wang M, Wang X, Gong F, Bai L, Zhang J and Wang W. Quantifying blood-brain-barrier leakage using a combination of evans blue and high molecular weight FITC-Dextran. J Neurosci Methods 2019; 325: 108349.
[26] Xu Q, Qaum T and Adamis AP. Sensitive blood-retinal barrier breakdown quantitation using Evans blue. Invest Ophthalmol Vis Sci 2001; 42: 789-794.
[27] Hjertkvist M and Bergh A. The time-response and magnitude of hCG-induced vascular

changes are different in scrotal and abdominal testes. Int J Androl 1993; 16: 63-70.
[28] Schumacher HR Jr. Synovial membrane and fluid morphologic alterations in early rheumatoid arthritis: microvascular injury and virus-like particles. Ann N Y Acad Sci 1975; 256: 39-64.
[29] Levick JR. Permeability of rheumatoid and normal human synovium to specific plasma proteins. Arthritis Rheum 1981; 24: 1550-1560.
[30] Rall LC, Rosen CJ, Dolnikowski G, Hartman WJ, Lundgren N, Abad LW, Dinarello CA and Roubenoff R. Protein metabolism in rheumatoid arthritis and aging. Effects of muscle strength training and tumor necrosis factor alpha. Arthritis Rheum 1996; 39: 1115-1124.
[31] Inglis JJ, Notley CA, Essex D, Wilson AW, Feldmann M, Anand P and Williams R. Collagen-induced arthritis as a model of hyperalgesia: functional and cellular analysis of the analgesic actions of tumor necrosis factor blockade. Arthritis Rheum 2007; 56: 4015-4023.
[32] Brand DD, Latham KA and Rosloniec EF. Collagen-induced arthritis. Nat Protoc 2007; 2: 1269-1275.
[33] Kuramoto Junior M, Matson E, Turbino ML and Marques RA. Microhardness of Nd:YAG laser irradiated enamel surfaces. Braz Dent J 2001; 12: 31-33.
[34] Oberg K, Modlin IM, De Herder W, Pavel M, Klimstra D, Frilling A, Metz DC, Heaney A, Kwekkeboom D, Strosberg J, Meyer T, Moss SF, Washington K, Wolin E, Liu E and Goldenring J. Consensus on biomarkers for neuroendocrine tumour disease. Lancet Oncol 2015; 16: e435-e446.
[35] Sanjay ST, Fu G, Dou M, Xu F, Liu R, Qi H and Li X. Biomarker detection for disease diagnosis using cost-effective microfluidic platforms. Analyst 2015; 140: 7062-7081.
[36] Brown PM, Pratt AG and Isaacs JD. Mechanism of action of methotrexate in rheumatoid arthritis, and the search for biomarkers. Nat Rev Rheumatol 2016; 12: 731-742.
[37] Najm A, Masson FM, Preuss P, Georges S, Ory B, Quillard T, Sood S, Goodyear CS, Veale DJ, Fearon U, Le Goff B and Blanchard F. MicroRNA-17-5p reduces inflammation and bone erosions in mice with collagen-induced arthritis and directly targets the JAK/STAT pathway in rheumatoid arthritis fibroblast-like synoviocytes. Arthritis Rheumatol 2020; 72: 2030-2039.
[38] Robinson WH and Mao R. Biomarkers to guide clinical therapeutics in rheumatology? Curr Opin Rheumatol 2016; 28: 168-175.
[39] Waterton JC, Ho M, Nordenmark LH, Jenkins M, DiCarlo J, Guillard G, Roberts C, Buonaccorsi G, Parker GJM, Bowes MA, Peterfy C, Kellner H and Taylor PC. Repeatability and response to therapy of dynamic contrast-enhanced magnetic resonance imaging biomarkers in rheumatoid arthritis in a large multicentre trial setting. Eur Radiol 2017; 27: 3662-3668.
[40] Xia W, Huang ZJ, Guo ZL, Feng YW, Zhang CY, He GY and Tang AZ. Plasma volume, cell volume, total blood volume and F factor in the tree shrew. PLoS One 2020; 15: e0234835.
[41] Wang Y, Lang L, Huang P, Wang Z, Jacobson O, Kiesewetter DO, Ali IU, Teng G, Niu G and Chen X. In vivo albumin labeling and lymphatic imaging. Proc Natl Acad Sci U S A 2015; 112: 208-213.
[42] Wick MJ, Harral JW, Loomis ZL and Dempsey EC. An optimized evans blue protocol to assess vascular leak in the mouse. J Vis Exp 2018; 57037.
[43] Li W, Ma N, Liu MX, Ye BJ, Li YJ, Hu HY and Tang YH. C1q/TNF-related protein-9 attenuates retinal inflammation and protects blood-retinal barrier in db/db mice. Eur J Pharmacol 2019; 853: 289-298.
[44] Dekker NAM, van Meurs M, van Leeuwen ALI, Hofland HM, van Slyke P, Vonk ABA, Boer C and van den Brom CE. Vasculotide, an angiopoietin-1 mimetic, reduces pulmonary vascular leakage and preserves microcirculatory perfusion during cardiopulmonary bypass in rats. Br J Anaesth 2018; 121: 1041-1051.
[45] Namykin AA, Shushunova NA, Ulanova MV, Semyachkina-Glushkovskaya OV, Tuchin VV and Fedosov IV. Intravital molecular tagging velocimetry of cerebral blood flow using Evans Blue. J Biophotonics 2018; 11: e201700343.
[46] Le VH and Fishman WH. Combination of Evans blue with plasma protein; its significance in capillary permeability studies, blood dye disappearance curves, and its use as a protein tag. Am J Physiol 1947; 151: 26-33.
[47] Fu Q, Zhu R, Song J, Yang H and Chen X. Photoacoustic imaging: contrast agents and their biomedical applications. Adv Mater 2019; 31: e1805875.
[48] Kim SH, Lee HS, Kang BJ, Song BJ, Kim HB, Lee H, Jin MS and Lee A. Dynamic contrast-enhanced MRI perfusion parameters as imaging biomarkers of angiogenesis. PLoS One 2016; 11: e0168632.
[49] Yoo SA, Kwok SK and Kim WU. Proinflammatory role of vascular endothelial growth factor in the pathogenesis of rheumatoid arthritis: prospects for therapeutic intervention. Mediators Inflamm 2008; 2008: 129873.
[50] Kaushik A, Jayant RD, Bhardwaj V and Nair M. Personalized nanomedicine for CNS diseases. Drug Discov Today 2018; 23: 1007-1015.

[51] Xie Z, Guo W, Guo N, Huangfu M, Liu H, Lin M, Xu W, Chen J, Wang T, Wei Q, Han M and Gao J. Targeting tumor hypoxia with stimulus-responsive nanocarriers in overcoming drug resistance and monitoring anticancer efficacy. Acta Biomater 2018; 71: 351-362.

[52] Xiao S, Tang Y, Lv Z, Lin Y and Chen L. Nanomedicine - advantages for their use in rheumatoid arthritis theranostics. J Control Release 2019; 316: 302-316.